Highly efficient spin-orbit torque in a perpendicular synthetic ferrimagnet

Zishuang Li,[1,*] Yining Fei,[1,*] Lina Chen,[1,2,†] Xiang Zhan,[1] Liupeng Yang,[1] Chunjie Yan,[1] Wenqiang Wang,[1] Kaiyuan Zhou,[1] Haotian Li,[1] Fusheng Ma,[3] Tiejun Zhou,[4,‡] Youwei Du,[1] and Ronghua Liu[1,§]

[1]*National Laboratory of Solid State Microstructures, School of Physics and Collaborative Innovation Center of Advanced Microstructures, Nanjing University, Nanjing 210093, China*

[2]*New Energy Technology Engineering Laboratory of Jiangsu Provence and School of Science, Nanjing University of Posts and Telecommunications, Nanjing 210023, China*

[3]*Jiangsu Key Laboratory of Opto-Electronic Technology, Center for Quantum Transport and Thermal Energy Science, School of Physics and Technology, Nanjing Normal University, Nanjing 210023, China*

[4]*Centre for Integrated Spintronic Devices, School of Electronics and Information, Hangzhou Dianzi University, Hangzhou 310018, China*

(Received 20 November 2021; revised 6 May 2022; accepted 6 May 2022; published 17 May 2022)

Perpendicular synthetic ferrimagnet (pSFi) due to the low stray field and net magnetization is expected to replace single ferromagnet as a free layer to optimize the memory devices for high storage density and low-energy consumption. Here, we investigate the dependence of exchange-coupling strength on the thickness of the spacer Ru and current-induced magnetization reversal due to spin-orbit torque in Ta/Pt/$[Pt/Co]_2$/Ru/$[Co/Pt]_4$/Pt structure with a perpendicular magnetic anisotropy. An oscillating interlayer exchange coupling as a function of Ru spacer layer thickness with a period of 1.16 nm is determined by combining the anomalous Hall effect and the polar magnetic-optical Kerr effect. Furthermore, current-controllable magnetization reversal experiments reveal that the magnetizations of top and bottom layers with antiferromagnetic coupling switch simultaneously due to the combination of spin-orbit torque generated from the two adjacent heavy-metal layers and the interlayer exchange torque. The SOT efficiency $\chi \sim 57.52\,\mathrm{Oe}/(10^6\,\mathrm{A/cm^2})$, corresponding to an effective spin Hall angle $\xi_{DL} \sim 0.68$, is estimated by analyzing current-dependent anomalous Hall resistance with our proposed quasistatic balance equation of magnetic moments. In addition to the advantage of minimizing stray field acting on the storage layer, the observed low switching current density and high spin-orbit torque efficiency suggest that the pSFi structure with a high thermal stability factor has great potential to realize the high-density and low-power consumption of nonvolatile magnetic memory devices.

DOI: 10.1103/PhysRevB.105.184419

I. INTRODUCTION

The magnetic tunnel junction (MTJ), due to its nonvolatility, high tunneling magnetoresistance ratio, and small size, has been widely used in magnetic sensor, storage, and logic devices, e.g., magnetic read head and magnetoresistive random access memory (MRAM) [1,2]. With massive data included in the current digital information, high-density and high-efficiency MRAM development based on various materials and structures has acquired increasing attention. In traditional MTJs, the free layer usually consists of a single ferromagnetic layer [3,4]. As the reduction of MTJ cell size or more MTJ cells are patterned into a smaller space, the local stray field generated from the ferromagnetic layer becomes the predominant factor, degrading the performance of MRAM [5,6]. Compared with ferromagnet, antiferromagnet with zero net magnetic moments as the free layer can eliminate or minimize the stray field. However, the characteristics of the antiferromagnet, being insensitive to the external magnetic field and charge current and challenging to experimental manipulation and detection, still impede the further application of antiferromagnet in MTJs [7]. Fortunately, the synthetic antiferromagnet (SAF) and synthetic ferrimagnet (SFi), consisting of two antiferromagnetically coupled ferromagnetic layers and a nonmagnetic spacer, possess the advantages of reduced stray field and high thermal stability due to the strong interlayer exchange coupling, as well as keeping almost the same manipulation and detection of magnetization as the single ferromagnet layer [8,9]. The interlayer exchange coupling between two magnetic layers adjacent to the same nonmagnetic spacer can be referred to as the Ruderman-Kittel-Kasuya-Yosida (RKKY) interaction [10,11]. Based on RKKY interaction theory, this sandwich structure has an oscillatory interlayer exchange coupling as a function of the nonmagnetic spacer layer thickness. Therefore, the interlayer exchange coupling provides an extra degree of freedom to manipulate dynamical modes that may reduce the switching time of MTJs. In the SAF film with such exchange-coupling torque, current-driven domain-wall motion can be more efficient with a faster speed of up to $\sim 750\,\mathrm{m/s}$ [12]. Recently, spin-orbit torque (SOT) has been brought up as a highly efficient and low-power consumption method to manipulate magnetization

*These authors contributed equally to this work.
†chenlina@njupt.edu.cn
‡tjzhou@hdu.edu.cn
§rhliu@nju.edu.cn

electronically [13–22]. Many experiments have been carried out in various systems, including simple NM/FM bilayers Pt/Co [13], Ta/CoFeB [14], TaO*x*/Py [18]; Bi-based topological insulators $(Bi_{0.5}Sb_{0.5})_2Te_3$ [23,24], Bi_2Se_3 [25,26]; and synthetic antiferromagnetic structures Co/Ru/[Co/Pt] [27], CoFeB/Ta/CoFeB [28], and Pt/Co/Ir multilayers [29], searching for promising systems with large SOT efficiency. SAF and SFi systems are potential candidates for high SOT efficiency, owing to the reduced stray field, interlayer exchange coupling, and probably additional sources of SOT from interfaces.

Although SOT in some SAF or SFi systems has been found experimentally [30,31], the quantitatively calculated SOT efficiency methods in the SAF and SFi structures are still insufficient and lack consistency. In this work, we systematically investigated the interlayer exchange-coupling (IEC) field and magnetic domain structure with different Ru thicknesses in $Ta/Pt/[Pt/Co]_2/Ru/[Co/Pt]_4/Pt$ films by combining anomalous Hall effect and the polar magnetic-optical Kerr effect techniques. We experimentally determined the optimum antiferromagnetic coupling thickness and the oscillating period of IEC. Two representative SFi films with different interlayer antiferromagnetic exchange-coupling fields were adopted to perform current-driven magnetization switching experiments. The magnetization switching critical current was lower than the single ferromagnet device. Furthermore, an alternative method of calculating the current-induced reduction of anomalous Hall resistance was proposed to quantify the SOT efficiency as high as $\chi = 57.52\,\mathrm{Oe}/(10^6\,\mathrm{A/cm^2})$, corresponding to an effective spin Hall angle $\xi_{DL} = 0.68$.

II. EXPERIMENT DETAILS

$Ta(4)/Pt(4)/[Pt(0.6)/Co(0.6)]_2/Ru(t_{Ru})/[Co(0.6)/Pt(0.6)]_4/Pt(1)$ multilayer stacks (from the bottom to the top, thickness in nanometers) were deposited on thermally oxidized $Si/SiO_2(300\,\mathrm{nm})$ substrates via DC magnetron sputtering at a base vacuum better than 2×10^{-8} Torr. The thickness t_{Ru} of Ru space layer is a range of 0–2.5 nm. The deposition pressure was $\sim 5.0 \times 10^{-3}$ Torr Ar. The deposition rates for each layer Pt$\sim$0.027 nm/s, Co$\sim$0.018 nm/s, Ru$\sim$0.015 nm/s, and Ta$\sim$0.024 nm/s were detected simultaneously using an *in situ* quartz crystal monitor. The studied devices were first patterned into Hall bar by combining electron-beam lithography and magnetron sputtering, as shown in Fig. 1(b). In the stack, the 4-nm-thick Ta layer was deposited as a buffer layer to improve surface smoothness and perpendicular magnetic anisotropy (PMA). When the charge current passes through the Hall bar, the spin current generated by the spin Hall effect (SHE) in the heavy-metal Pt would flow upward, exert spin-orbit torque on magnetic moments, and switch the magnetization of the Pt/Co multilayer. We adopted Co/Pt multilayers with different numbers as bottom and top FM layers for our experimental distinction between two FM layers. The magnetic properties of samples were characterized by polar magneto-optical Kerr effect (PMOKE) [32,33] and anomalous Hall effect (AHE) [34] measurements in the patterned Hall cross.

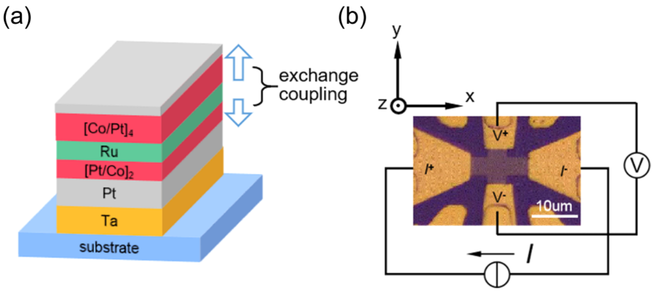

FIG. 1. (a) Schematic of a $Ta/Pt/[Pt/Co]_2/Ru/[Co/Pt]_4/Pt$ multilayer. (b) The optical microscope image of the Hall bar and the measurement configuration of anomalous Hall resistance.

III. RESULTS AND DISCUSSION

A. Interlayer exchange coupling

We first show the out-of-plane hysteresis of the heterostructures with different thicknesses of Ru spacer measured by PMOKE. Figure 2(a) shows that the PMOKE hysteresis loops exhibit a well-defined square shape under an out-of-plane magnetic field, similar to a single FM layer with strong PMA, indicating the magnetic moments of the bottom and upper [Co/Pt] multilayers with the labeled thicknesses of Ru spacer arrange parallelly with an interlayer ferromagnetic coupling. The coercive field H_c generally decreases with increasing thickness t_{Ru} of Ru spacer, resulting from the reduction in the interlayer exchange coupling and PMA of the upper [Co/Pt] layer, which depends on the thickness of the spacer (or buffer) layer Ru [35]. The PMOKE images also confirmed that [Co/Pt] multilayers exhibit a single-domain structure. However, Fig. 2(b) shows several separate switching fields with four intensity plateaus, suggesting the bottom and upper magnetic layers have an interlayer AFM exchange coupling for the labeled thicknesses of Ru spacer. The corresponding PMOKE images also indicate that [Co/Pt] multilayers form a single-domain structure.

To better illustrate the magnetization switching process of the bottom and upper layers, we adopt two representative AHE hysteresis loops corresponding to FM exchange coupling ($t_{Ru} = 1.5\,\mathrm{nm}$) [Fig. 2(c)] and AFM ($t_{Ru} = 1\,\mathrm{nm}$) [Fig. 2(d)] exchange coupling, respectively, with the external out-of-plane magnetic field and a small DC current of 0.5 mA. For the $t_{Ru} = 1.5\,\mathrm{nm}$ sample, like the PMOKE hysteresis loop, Fig. 2(c) shows a single hysteresis loop, suggesting that the parallel magnetizations of the top and bottom layers switch together at the coercive field due to strong interlayer FM exchange coupling and non-negligible dipolar interaction. For the $t_{Ru} = 1.0\,\mathrm{nm}$ sample, Fig. 2(d) shows four states forming three loops with the same Hall resistance difference value ΔR_H. Since anomalous Hall resistance R_H is proportion to the magnetization and thickness of the magnetic layer, ΔR_H contributed from the upper $[Pt/Co]_4$ layer is twice as high as from the bottom $[Pt/Co]_2$ layer. Therefore, the minor loops at high magnetic field represent the magnetization switching of the bottom $[Pt/Co]_2$ layer, and the field shift of the minor loop is defined as the antiferromagnetic exchange coupling field $H_{IEC,b}$ experienced by the bottom FM layer (denoted as H_{IEC} below for simplicity). The prime loop at the low magnetic

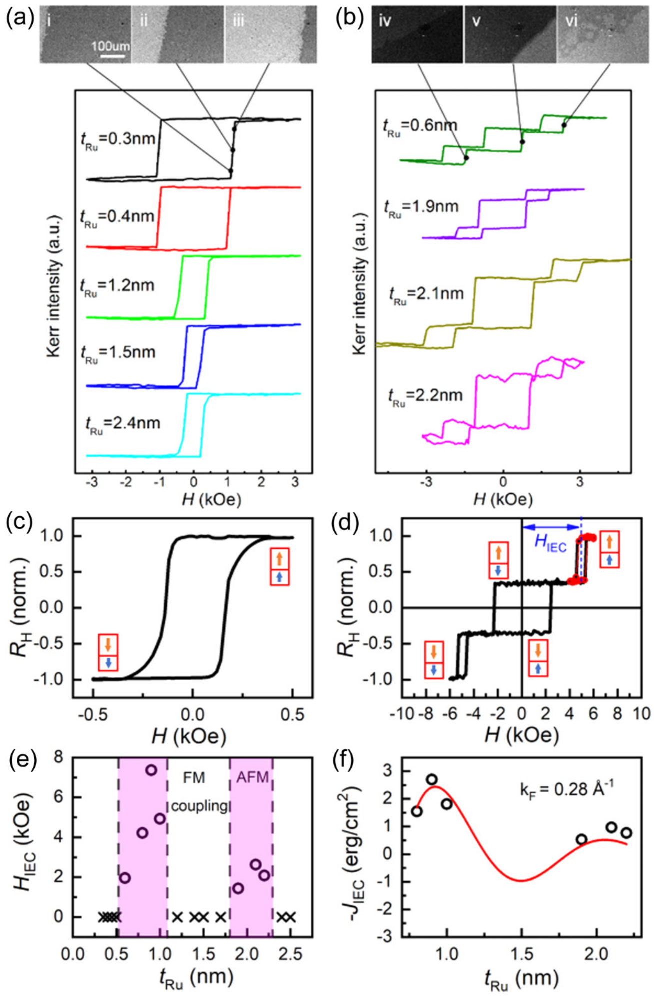

FIG. 2. (a), (b) Out-of-plane PMOKE hysteresis loops of the samples with FM (a) and AFM (b) interlayer exchange coupling. The top inset PMOKE images show magnetic domain structures during the field-driven magnetization switching process. The thickness of the Ru spacer is labeled. (c), (d) Normalized out-of-plane AHE hysteresis loop for samples with 1.5-nm- (c) and 1.0-nm- (d) thick Ru spacer. The blue and orange arrows depict the bottom and the upper magnetic moments. (e) Dependence of interlayer exchange-coupling field on thickness t_{Ru} of Ru spacer. The crosses represent the FM coupling samples. (f) The interlayer exchange-coupling strength J_{IEC} vs t_{Ru}. The solid curve is the RKKY formula fitting result.

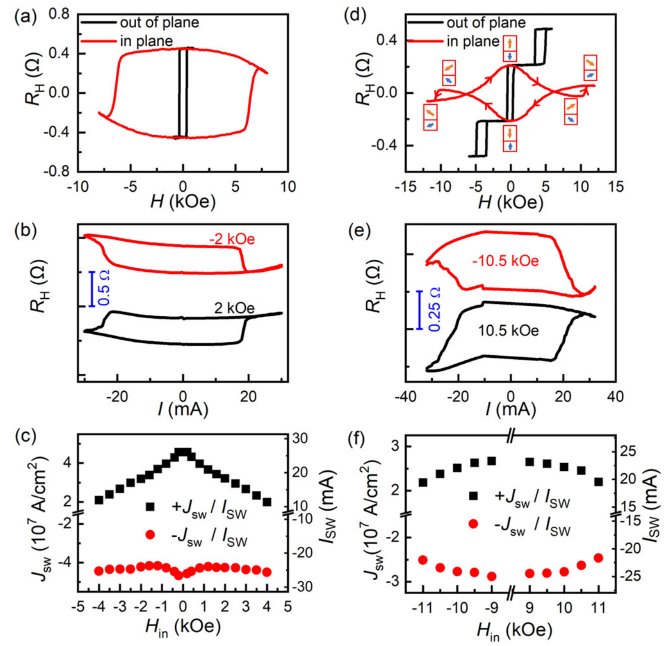

FIG. 3. (a), (d) Anomalous Hall resistance R_H hysteresis loops of Ta/Pt/[Pt/Co]$_2$/Ru control sample with only bottom magnetic layer (a) and $t_{Ru} = 1.0$-nm SFi sample (d) measured with a small DC current $I = 0.5$ mA under out-of-plane (black curve) and in-plane (red curve) magnetic fields. The arrows in (d) illustrate the magnetic moments' orientations of bottom and upper FM layers under an in-plane field. (b), (e) Current-induced switching of Ta/Pt/[Pt/Co]$_2$/Ru (b) and $t_{Ru} = 1.0$-nm SFi sample (e) under the labeled in-plane external fields H_{out} in the direction of the current. (c), (f) The critical switching current density J_c vs H_{in} for Ta/Pt/[Pt/Co]$_2$/Ru (c) and $t_{Ru} = 1.0$-nm SFi sample (f), respectively.

field represents the switching between the two antiferromagnetic states ("↑↓" and "↓↑", denoted as the "tail-to-tail" and "head-to-head" state, respectively), as illustrated in Fig. 2(d). In terms of energy, the parallel or antiparallel configurations of this studied magnetic sandwich structure are dominated by PMA, Zeeman energy, and interlayer exchange coupling [36]. When the external out-of-plane magnetic field is larger than the interlayer exchange-coupling field, the Zeeman energy becomes dominant, and magnetizations of both layers are along the external magnetic field. In contrast, when the external magnetic field is smaller than H_{IEC}, magnetizations of two layers are antiparallel, and magnetization of the upper thick [Co/Pt]$_4$ layer is parallel to the external magnetic field. Therefore, from the negative magnetic field to the positive magnetic field, the four states are in the sequence of "↓↓", "↑↓", "↓↑," and "↑↑" [inset in Fig. 3(d)].

The experimentally determined interlayer exchange-coupling field H_{IEC} of all samples with different thicknesses t_{Ru} of Ru spacer were summarized in Fig. 2(e), where the FM and AFM exchange coupling vary alternatively and decay with the increase of t_{Ru}. The spacer thickness with $0.5\,\text{nm} \leqslant t_{Ru} \leqslant 1.0\,\text{nm}$ and $1.8\,\text{nm} \leqslant t_{Ru} \leqslant 2.4\,\text{nm}$ correspond to the first and second AFM coupling regimes, respectively. The first peak of AFM coupling occurs at $t_{Ru} \sim 0.9\,\text{nm}$ with H_{IEC} up to 7.3 kOe and the second peak at $t_{Ru} \sim 2.1\,\text{nm}$ with H_{IEC} up to 2.2 kOe. This oscillating interlayer exchange interaction is well consistent with an RKKY indirect exchange interaction [37]. This interlayer exchange-coupling strength for different thicknesses of Ru can be calculated by the equation $J_{IEC} = H_{IEC} M_s t_{FM}$ [38], where M_s and t_{FM} are the saturation magnetization and thickness of the bottom [Pt/Co]$_n$ multilayer, respectively. Furthermore, we adopted Yafet's RKKY model [39], considering two-dimensional layers with a uniform distribution of spins. The spins within a layer are assumed to be aligned in parallel, and the interlayer coupling strength is in the form $J \sim Y(2k_F t)$, where $Y(x) = \frac{x\cos x - \sin x}{2x^2} - \frac{1}{2}\int_x^\infty \frac{\sin y}{y} dy$, and k_F and t are the Fermi wave vector involved in the RKKY coupling and thickness of the Ru spacer, respectively. The second term of an oscillatory integration is neglected in fitting. The result gives $k_F = 0.28\,Å^{-1}$, which is consistent with Zhao *et al.*'s work [40].

B. Current-driven magnetization reversal of SFi

Now we study current-induced SOT-driven magnetization switching in the AFM coupling samples. We also prepared a Ta/Pt/$[Pt/Co]_2$/Ru device with only the bottom FM layer as a control group towards the studied SFi devices. Figure 3(a) presents the AHE hysteresis loops of the control sample under in-plane and out-of-plane magnetic fields, which exhibit a square loop indicating a well-defined PMA. Figure 3(b) records the anomalous Hall resistance during the scanning of a current I along the long side of the Hall bar under a fixed external magnetic field of ± 2 kOe parallel to the current (along the x axis). The switching polarity changes as the in-plane magnetic field direction reverses, consistent with the symmetry of current-induced SOT due to spin Hall and interfacial Rashba effects [41]. It is worth mentioning that the sweeping current started from the positive side in Fig. 3(b) and the first switching at negative current is incomplete, as the anomalous Hall resistance difference $\triangle R_H$ is about one-half of that in the field-driven AHE measurement in Fig. 3(a). As a result, the switching at positive current occurred earlier, leading to the asymmetry of critical switching current shown in Fig. 3(c).

For the Ta/Pt/$[Pt/Co]_2$/Ru/$[Co/Pt]_4$/Pt SFi sample with $t_{Ru} = 1.0$ nm, the representative AHE hysteresis loops and the SOT switching curves are presented in Fig. 3(d) and Fig. 3(e), respectively. The perpendicular interlayer exchange-coupling field H_{IEC} is 4.7 kOe, obtained from the AHE hysteresis loop with the out-of-plane magnetic field. Meanwhile, when the applied in-plane magnetic field along the x axis reaches about 10.7 kOe, both magnetizations of the bottom and the upper FM layers switch to near parallel with the direction of the external magnetic field, as shown in Fig. 3(d). Combining the AHE hysteresis loops and the current-induced SOT switching loops [Fig. 3(e)], we conclude that the magnetization configurations consisting of two FM layers with interlayer AFM coupling are switching between the head-to-head and the tail-to-tail antiferromagnetic states. In the studied SFi sample, the current-induced SOT, mainly generated from the thick bottom Pt layer, acts on its adjacent bottom $[Pt/Co]_2$ layer and then drives the magnetization switching of the upper $[Co/Pt]_4$ layer through the dipolar interaction between layers and the interlayer AFM coupling-induced effective IEC field [29].

The critical switching current I_{sw} is defined by the current value where the R_H has a 50% switching magnitude in Fig. 3(b) and Fig. 3(e). Figure 3(c) and Fig. 3(f) show that although the thickness of the total magnetic layer in the SFi device is three times that of the FM layer in the control sample, the SFi device still has a comparable I_{sw} value with the single FM device. To straightforwardly compare the current-driven magnetization switching power efficiency between the FM- and SFi-based SOT devices, the critical switching current density J_{sw} was calculated by assuming the applied current flows uniformly in the Hall bar. The J_{sw} of the SFi device is 2.1×10^7–2.7×10^7 A/cm^2 under the studied in-plane magnetic fields, slightly lower than 3×10^7–4×10^7 A/cm^2 of the single FM control sample. If further considering the current shunting effect arising from the magnetic layer, the J_{sw} in the heavy-metal layers for the SFi device will be much lower than the single FM device. The significant reduction of the critical current density for the SFi device is expected to the additional current-induced SOT exerting on the upper $[Co/Pt]_4$ layer generated by the top 1-nm-thick Pt layer. As we know, the spin polarization of the spin currents generated from the bottom and top Pt layers are opposite. Moreover, the magnetizations of the bottom and the upper FM layers in the SFi device are antiparallel. Therefore, the bottom and top Pt layers-induced SOTs in the SFi device should be added and significantly reduce J_{sw}.

C. Estimation of current-induced SOT efficiency

The SOT efficiency is a critical factor related to the power consumption and operation speed of the magnetic memory device. It can be quantitatively characterized by the SOT-induced effective magnetic field H_{eff}. Here, we will introduce an alternative way from previously reported methods [31,42,43] to characterize current-induced H_{eff} by analyzing current-dependent anomalous Hall resistance R_H under a large out-of-plane magnetic field measurement geometry. Figure 4(a) shows the AHE hysteresis loop of the $t_{Ru} =$ 2.0 nm SFi sample with a relatively weak interlayer AFM coupling $H_{IEC} \sim 1.57$ kOe. Since AHE is proportional to the z component of the magnetization, the anomalous Hall resistivity can be expressed by $\rho_H = 4\pi(R_s^b M_z^b + R_s^u M_z^u)$ [34], where R_s^b, M_z^b, R_s^u, and M_z^u are the anomalous Hall coefficient and the z component of the magnetization of the bottom and upper FM layer, respectively. Based on the resistance change between the antiferromagnetic state and ferromagnetic state, we find that the anomalous Hall resistance follows a relation of $R_H^b : R_H^u = 2 : 3$, where R_H^b and R_H^u are the anomalous Hall resistance contributed by the bottom FM and the upper FM layers, respectively. This ratio could attribute to the stronger spin-orbit coupling at the interfaces of Pt(4)/$[Pt/Co]_2$/Ru(2) for the bottom FM layer and Ru(2)/$[Pt/Co]_4$/Pt(1) for the upper FM layer due to the different thickness of Pt and the different stacking order of FM, Pt, and Ru [44]. The SOT switching curves with the various in-plane magnetic fields and the critical current density are also presented in Fig. 4(b) and Fig. 4(c). Compared to the $t_{Ru} =$ 1-nm SFi device with a large interlayer AFM coupling $H_{IEC} \sim 4.85$ kOe, the $t_{Ru} =$ 2-nm device exhibits a relatively low $J_{sw} = 14.5 \times 10^6$–$23.2 \times 10^6$ A/cm^2 and a very small assistant in-plane magnetic field $H_{in}^{min} \sim 0.5$ kOe.

Figure 5(a) shows the current-dependent AHE hysteresis loops under different out-of-plane magnetic fields. The current is swept between 27 and -27 mA under different H_{out} varied from 3 to -3 kOe. Unlike the above current-dependent AHE hysteresis loop with inversion symmetry under in-plane fields, R_H vs I curves under the out-of-plane fields show symmetry and no hysteretic behavior. For instance, when the out-of-plane field of $H_{out} = 3$ kOe is applied, we find that magnetizations of both FM layers in SFi under small currents are forced to align parallel to the external field by directly comparing the value of R_H between R_H vs I and

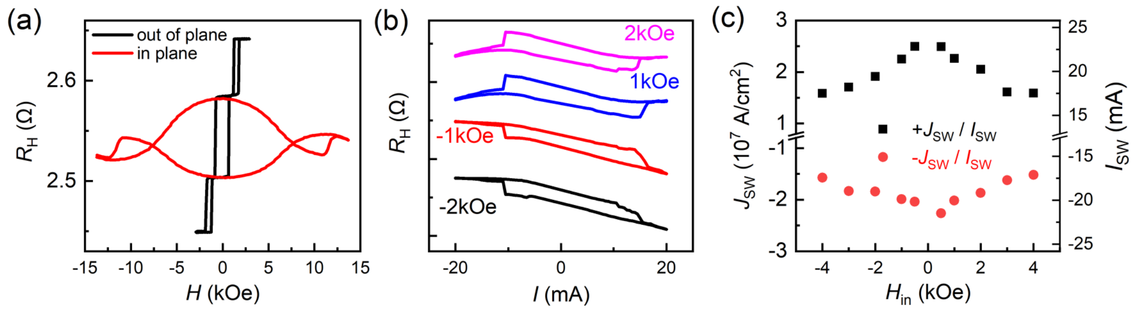

FIG. 4. Current-induced magnetization switching of the AFM coupling sample $t_{\rm Ru} = 2\,\rm nm$ under an in-plane magnetic field. (a) Field-dependent $R_{\rm H}$ hysteresis loops measured with an out-of-plane magnetic field and a small DC current $I = 0.5\,\rm mA$. (b) DC current-dependent $R_{\rm H}$ hysteresis loops measured with different in-plane magnetic field $H_{\rm in}$ along the direction of applied current. (c) The critical switching current $J_{\rm c}$ vs in-plane $H_{\rm in}$.

$R_{\rm H}$ vs $H_{\rm out}$ loops [Fig. 4(a)]. However, the $R_{\rm H}$ shows a significant decrease with increasing current because current-induced dampinglike spin-orbit torque tilts the magnetic moments in the FM layer due to the spin Hall and interfacial Rashba effects. $H_{\rm eff} = \sigma \times M$ is perpendicular to the magnetization direction (as σ, denoting the polarization of the spin current generated by the Pt layer, aligns on the y axis and M on the z axis) and causes the reduction of the z component of the magnetization and $R_{\rm H}$ in SFi. The bottom and upper Pt layers generate spin currents and exert SOTs on their adjacent FM layers. However, considering the spin-diffusion model [45] and different thicknesses of the bottom ($t_b = 4.6\,\rm nm$) and upper Pt layers ($t_u = 1.6\,\rm nm$), the current-induced effective magnetic field on the bottom FM layer is much larger than the upper FM layer.

To quantitatively calculate the SOT-induced $H_{\rm eff}$, we first need to preprocess the raw $R_{\rm H}(I)$ data in Fig. 5(a). When $H_{\rm out}$ is lower than $H_{\rm IEC} = 1.57\,\rm kOe$ with small currents, magnetizations in SFi prefer a perpendicular antiparallel configuration, consistent with the $R_{\rm H}$ vs I curves below 15 mA obtained at $H_{\rm out} < 1\rm kOe$, while $H_{\rm out} > H_{\rm IEC} = 1.57\,\rm kOe$, the bottom and upper FM layers are parallel to the external field. Thus, we choose the $R_{\rm H}$ curve obtained at $H_{\rm AP} = H_{\rm out} = 0.1\,\rm kOe$ as the reference to remove the background signals consisting of longitudinal resistance and other systematic noise, and extract the current-induced deviation of the $R_{\rm H}$ at high fields. For better mathematical representations and convenience of analysis, we rewrite the anomalous Hall resistance of the bottom FM layers as follows:

$$\begin{aligned}\Delta R_{\rm H} &= R_{\rm H}(I,\ H_{\rm P}) - R_{\rm H}(I,\ H_{\rm AP})\\ &= \left[R_{\rm H}^{\rm u}(I,\ H_{\rm P}) + R_{\rm H}^{\rm b}(I, H_{\rm P})\right]\\ &\quad - \left[R_{\rm H}^{\rm u}(I, H_{\rm AP}) - R_{\rm H}^{\rm b}(I, H_{\rm AP})\right]\\ &= R_{\rm H0}^{\rm u}\left(\cos\theta_{\rm P}^{\rm u} - \cos\theta_{\rm AP}^{\rm u}\right) + R_{\rm H0}^{\rm b}\left(\cos\theta_{\rm P}^{b} + \cos\theta_{\rm AP}^{b}\right), \quad (1)\end{aligned}$$

where θ is the tilting angle of the magnetic moments from the normal direction of the film and is confined in $-90^\circ\sim 90^\circ$. The superscripts u, b represent the upper FM layer and the bottom, the subscripts P, AP represent parallel state and antiparallel state, respectively. $R_{\rm H0}^{\rm u} \sim 0.170\ \Omega$ and $R_{\rm H0}^{\rm b} \sim 0.115\ \Omega$ are the anomalous Hall resistance of each layer with their magnetic moments along the normal direction of film at room temperature, determined from the out-of-plane AHE loop in Fig. 4(a). If taking into account the Joule heating effect on the magnetization of the FM layer under a large current, we include an additional current modification of $R_{\rm H}^{\rm u,b} = R_{\rm H0}^{\rm u,b}(1 - \beta J^2)$, where β is a relevant heating effect coefficient. Combined with the balance condition of magnetization of each layer $\boldsymbol{M} \times (\boldsymbol{H}_{\bf out} + \boldsymbol{H}_{\bf k} - \boldsymbol{H}_{\bf IEC}) = \boldsymbol{M} \times \boldsymbol{H}_{\bf eff}$, the external out-of-plane field $H_{\rm out}$, effective PMA field $H_{\rm k}$, interlayer exchange-coupling field $H_{\rm IEC}$, and SOT effective field $H_{\rm eff}$ are

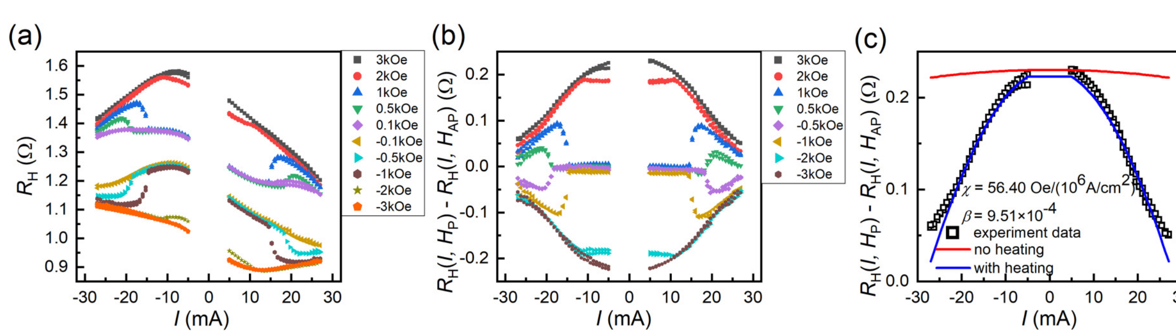

FIG. 5. Quantitative analysis of the current-induced SOT effective field of the AFM coupling sample $t_{\rm Ru} = 2\,\rm nm$. (a) The raw current-dependent anomalous Hall resistance $R_{\rm H}$ under a series of out-of-plane magnetic fields. The raw $R_{\rm H}(I)$ includes a significant background noise consisting of the longitudinal resistance due to asymmetrically manufactured lateral electrodes, the Joule heating effect, and other systematic noise. (b) The difference of $R_{\rm H}$ between the parallel state at high fields and the antiparallel state at the low field, $H_{\rm out} = 0.1\,\rm kOe$. (c) Experimental data (symbol) and numerical fitting curves (solid lines) under $H_{\rm out} = 3\,\rm kOe$.

TABLE I. Calculated results of the effective SOT efficiency $\chi = H_{\text{eff}}/J$, the effective PMA field H_k, the IEC field H_{IEC}, and the heating effect coefficient β.

Experiment R_H vs I curves	$\beta(\times 10^{-4})$	χ [Oe/(10^6 A/cm^2)]
$H_{\text{out}} = 3$ kOe	9.51	56.40
$H_{\text{out}} = -3$ kOe	9.41	58.64
Average values	9.46	57.52

canceled out. Considering that H_{out} and H_k are perpendicular to the sample film plane, H_{IEC} is antiparallel to the other FM layer, H_{eff} is perpendicular to the magnetic moments, and the vector balance equation can be reduced to a scalar form:

$$H_{\text{out}}\sin\theta_P^u + H_k^u\cos\theta_P^u\sin\theta_P^u - H_{\text{IEC}}^u\sin\left(\theta_P^u + \theta_P^b\right) = H_{\text{eff}}^u, \quad (2)$$

$$H_{\text{out}}\sin\theta_P^b + H_k^b\cos\theta_P^b\sin\theta_P^b - H_{\text{IEC}}^b\sin\left(\theta_P^u + \theta_P^b\right) = H_{\text{eff}}^b, \quad (3)$$

$$H_{\text{out}}\sin\theta_{AP}^u + H_k^u\cos\theta_{AP}^u\sin\theta_{AP}^u - H_{\text{IEC}}^u\sin\left(\theta_{AP}^u - \theta_{AP}^b\right) = H_{\text{eff}}^u, \quad (4)$$

$$H_{\text{out}}\sin\theta_{AP}^b + H_k^b\cos\theta_{AP}^b\sin\theta_{AP}^b - H_{\text{IEC}}^b\sin\left(\theta_{AP}^u - \theta_{AP}^b\right) = H_{\text{eff}}^b. \quad (5)$$

We determined the effective PMA field of the bottom FM layer $H_k^b = 5.69$ kOe by fitting the in-plane AHE hysteresis loop of Ta/Pt/[Pt/Co]$_2$/Ru control sample by the equation $\frac{R_H}{R_{H0}} = \frac{H}{\sqrt{H^2+H_k{}^2}}$. The overall PMA field of the SFi sample including the bottom and top FM layers was estimated by the area difference between the in-plane and out-of-plane magnetization loop [46], and then the effective PMA field of the upper FM layer $H_k^u = 2.10$ kOe was able to be deducted. The result shows that despite a relatively thick Ru spacer inserted between the upper and the bottom Co/Pt multilayers, the upper one still exhibits a considerable PMA and the SFi sample shows an overall PMA [Fig. 4(a)], consistent with the previous reports [46,47]. Considering the spin-diffusion model [45], the effective spin Hall angle is expressed by $\xi_{DL} = \theta_{DL}[1 - \text{sech}(t_{Pt}/\lambda_{SF})]$, where θ_{DL} is the intrinsic spin Hall angle of heavy metal. Taking the spin-diffusion length of Pt as 1.4 nm [14], the thickness is 1.6 and 4.6 nm for the upper and bottom Pt layers, respectively. Therefore, the ξ_{DL} of the upper Pt layer is about 4/9 of the bottom one and so is the effective SOT efficiency.

Figure 5(c) shows the calculation result vs the experiment data, which is numerically solved by the balance equation under $H_{\text{out}} = 3$ kOe with (solid red line) and without (solid blue line) considering the Joule heating effect. The obtained effective SOT efficiency $\chi = H_{\text{eff}}/J$ is summarized in Table I, where J is the current density of the total multilayer, calculated by assuming a uniform current density distribution.

From Table I, the SOT efficiency in our SFi sample with $t_{Ru} = 2.0$ nm reaches ~ 57.52 Oe/(10^6 A/cm^2), much higher than the previously reported value of 22 Oe/(10^6 A/cm^2) in the SAF Pt/[Co/Pd/Co]/Ru/[Co/Pd/Co] only with single Pt layer [31] and one order larger than 7.5 Oe/(10^6 A/cm^2) in the single ferromagnetic Pt/Co/MgO system [42]. In these previous works, the quantitative calculation method of the SOT efficiency follows the scenario that magnetization-switching behavior is caused by current-induced magnetic domain-wall motion. The Pt/FM with strong interfacial PMA and Dzyaloshinskii-Moriya interaction tends to form the Néel-type domain walls, where the magnetization moments in the domain wall are in the film plane so that the current-induced SOT effective field on the domain wall is perpendicular to the film plane. Opposite currents would facilitate or hinder domain-wall motion, resulting in the shift of the coercive field [42,43]. As a comparison, our method is based on the quasistatic process of the magnetization balance under the several external fields and the current-induced SOT effective field. In our measurement configuration, the upper and bottom FM layers are forced to a single domain by the large external out-of-plane field. Both the upper and bottom Pt layers inject spin currents with opposite polarity, tilting magnetizations of the adjacent FM layers and causing the reduction in anomalous Hall resistance. In addition, our method can avoid the complicated interference to the first- and second-harmonic Hall resistances under in-plane magnetic field measurement configuration caused by current-induced magnetic domain motion in the electrical heterodyne detection of current-induced SOT effective field [48–50]. For convenient comparison, we also calculated the effective spin Hall angle given by $\chi = \frac{\pi}{2}\frac{\hbar\xi_{DL}}{2e\mu_0 M_s t_{FM}}$ [42], where M_s is the saturated magnetization, t_{FM} is the thickness of FM layer, ξ_{DL} is the effective spin Hall angle; as well, $\hbar$, e, and μ_0 are the Planck constant, elementary charge, and vacuum permeability, respectively. In our $t_{Ru} = 2.0$-nm SFi sample, $t_{FM} = 0.6$ nm and $M_s = 1020$ emu/cm^3, $\chi = 57.52$ Oe/(10^6 A/cm^2), and the calculated ξ_{DL} from the above formula is $\sim$0.68, also larger than the previously reported $\xi_{DL} \sim 0.47$ in completely compensated SAF system [31]. The different calculating models based on distinct physical scenarios obtain a slightly larger value of ξ_{DL} in the different Pt-based SAF systems, indicating the validity of our calculating model based on our proposed balance equation of magnetization under the out-of-plane field geometry. Moreover, our results demonstrate that using bottom and top Pt layers adjacent to the AFM coupling two FM layers in the SFi can significantly enhance current-induced effective SOT efficiency and provide a simple, easy method to implement and feasible approach for the development of energy-efficient SFi-based spin-orbitronics.

IV. CONCLUSIONS

In summary, we experimentally determined the oscillating interlayer exchange coupling as a function of Ru spacer-layer thickness with a period of 1.16 nm in a Ta/Pt/[Pt/Co]$_2$/Ru(t_{Ru})/[Co/Pt]$_4$/Pt stacked multilayer with a strong perpendicular magnetic anisotropy. Furthermore, in the first ($t_{Ru} = 1$ nm) and the second ($t_{Ru} = 2$ nm) interlayer AFM coupling regime SFi multilayers, we demonstrated current-induced SOT-driven magnetization reversal between the two antiferromagnetic states. From the critical switching current directly compared with the single FM control sample and quantitative calculation of SOT-induced dampinglike effective field, our results suggest that the double enhancement of current-induced SOT efficiency generated by the high-conductivity Pt could be achieved through combining antiparallel magnetization configuration due to interlayer AFM coupling and opposite spin polarization at the bottom and top surfaces of Pt. Our results demonstrate that the SFi-based spin-orbitronics will be a practical approach to developing high-density, low-power consumption, fast-speed, high-durability nonvolatile memory devices because it possesses several advantages of reduced stray field, low critical operation current, and high thermal stability.

ACKNOWLEDGMENTS

This project was supported by the National Natural Science Foundation of China (Grants No. 11874135, No. 12074178, No. 12004171, and No. 12074189), the Applied Basic Research Programs of Science and Technology Commission Foundation of Jiangsu Province, China (Grant No. BK20200309), the Open Research Fund of Jiangsu Provincial Key Laboratory for Nanotechnology, the Scientific Foundation of Nanjing University of Posts and Telecommunications (NUPTSF) (Grant No. NY220164), and Key Research and Development Program of Zhejiang Province (Grant No. 2021C01039).

[1] G. Reiss, J. Schmalhorst, A. Thomas, A. Huetten, and S. Yuasa, in *Magnetic Heterostructures: Advances and Perspective in Spinstructures and Spintransport*, edited by H. Zabel and S. D. Bader (Springer-Verlag, Berlin, 2008), pp. 291.

[2] S. Ikeda, K. Miura, H. Yamamoto, K. Mizunuma, H. D. Gan, M. Endo, S. Kanai, J. Hayakawa, F. Matsukura, and H. Ohno, A perpendicular-anisotropy CoFeB-MgO magnetic tunnel junction, Nat. Mater. **9**, 721 (2010).

[3] S. S. P. Parkin, K. P. Roche, M. G. Samant, P. M. Rice, R. B. Beyers, R. E. Scheuerlein, E. J. O'Sullivan, S. L. Brown, J. Bucchigano, D. W. Abraham, Y. Lu, M. Rooks, P. L. Trouilloud, R. A. Wanner, and W. J. Gallagher, Exchange-biased magnetic tunnel junctions and application to nonvolatile magnetic random access memory (invited), J. Appl. Phys. **85**, 5828 (1999).

[4] Z. T. Diao, Z. J. Li, S. Y. Wang, Y. F. Ding, A. Panchula, E. Chen, L. C. Wang, and Y. M. Huai, Spin-transfer torque switching in magnetic tunnel junctions and spin-transfer torque random access memory, J. Phys.: Condens. Matter **19**, 165209 (2007).

[5] D. Houssameddine, J. F. Sierra, D. Gusakova, B. Delaet, U. Ebels, L. D. Buda-Prejbeanu, M. C. Cyrille, B. Dieny, B. Ocker, J. Langer, and W. Maas, Spin torque driven excitations in a synthetic antiferromagnet, Appl. Phys. Lett. **96**, 072511 (2010).

[6] Q. Y. Li, P. H. Zhang, H. T. Li, L. N. Chen, K. Y. Zhou, C. J. Yan, L. Y. Li, Y. B. Xu, W. X. Zhang, B. Liu, H. Meng, R. H. Liu, and Y. W. Du, Experiments and SPICE simulations of double MgO-based perpendicular magnetic tunnel junction, Chin. Phys. B **30**, 047504 (2021).

[7] C. Song, Y. F. You, X. Z. Chen, X. F. Zhou, Y. Y. Wang, and F. Pan, How to manipulate magnetic states of antiferromagnets, Nanotechnology **29**, 112001 (2018).

[8] R. A. Duine, K. J. Lee, S. S. P. Parkin, and M. D. Stiles, Synthetic antiferromagnetic spintronics, Nat. Phys. **14**, 217 (2018).

[9] W. Wang, P. Li, C. Cao, F. Liu, R. Tang, G. Chai, and C. Jiang, Temperature dependence of interlayer exchange coupling and Gilbert damping in synthetic antiferromagnetic trilayers investigated using broadband ferromagnetic resonance, Appl. Phys. Lett. **113**, 042401 (2018).

[10] L. C. Andreani, S. Fraizzoli, and H. Beck, Competition between Kondo effect and RKKY interaction: A molecular model, Solid State Commun. **77**, 635 (1991).

[11] P. Bruno, Theory of interlayer magnetic coupling, Phys. Rev. B **52**, 411 (1995).

[12] S. H. Yang, K. S. Ryu, and S. Parkin, Domain-wall velocities of up to 750 m/s driven by exchange-coupling torque in synthetic antiferromagnets, Nat. Nanotechnol. **10**, 221 (2015).

[13] I. M. Miron, K. Garello, G. Gaudin, P.-J. Zermatten, M. V. Costache, S. Auffret, S. Bandiera, B. Rodmacq, A. Schuhl, and P. Gambardella, Perpendicular switching of a single ferromagnetic layer induced by in-plane current injection, Nature (London) **476**, 189 (2011).

[14] L. Liu, T. Moriyama, D. C. Ralph, and R. A. Buhrman, Spin-Torque Ferromagnetic Resonance Induced by the Spin Hall Effect, Phys. Rev. Lett. **106**, 036601 (2011).

[15] L. Liu, C.-F. Pai, Y. Li, H. W. Tseng, D. C. Ralph, and R. A. Buhrman, Spin-torque switching with the giant spin Hall effect of tantalum, Science **336**, 555 (2012).

[16] X. Fan, H. Celik, J. Wu, C. Y. Ni, K. J. Lee, V. O. Lorenz, and J. Q. Xiao, Quantifying interface and bulk contributions to spin-orbit torque in magnetic bilayers, Nat. Commun. **5**, 3042 (2014).

[17] X. P. Qiu, Z. Shi, W. J. Fan, S. M. Zhou, and H. Yang, Characterization and manipulation of spin orbit torque in magnetic heterostructures, Adv. Mater. **30**, 1705699 (2018).

[18] L. P. Yang, Y. N. Fei, K. Y. Zhou, L. N. Chen, Q. W. Fu, L. Y. Li, C. J. Yan, H. T. Li, Y. W. Du, and R. H. Liu, Maximizing spin-orbit torque efficiency of Ta(O)/Py via modulating oxygen-induced interface orbital hybridization, Appl. Phys. Lett. **118**, 032405 (2021).

[19] C. Song, R. Q. Zhang, L. Y. Liao, Y. J. Zhou, X. F. Zhou, R. Y. Chen, Y. F. You, X. Z. Chen, and F. Pan, Spin-orbit torques: Materials, mechanisms, performances, and potential applications, Prog. Mater. Sci. **118**, 100761 (2021).

[20] R. H. Liu, W. L. Lim, and S. Urazhdin, Control of current-induced spin-orbit effects in a ferromagnetic heterostructure by electric field, Phys. Rev. B **89**, 220409(R) (2014).

[21] X. Qiu, W. Legrand, P. He, Y. Wu, J. Yu, R. Ramaswamy, A. Manchon, and H. Yang, Enhanced Spin-Orbit Torque Via Modulation of Spin Current Absorption, Phys. Rev. Lett. **117**, 217206 (2016).

[22] Z. Zheng, Y. Zhang, X. Feng, K. Zhang, J. Nan, Z. Zhang, G. Wang, J. Wang, N. Lei, D. Liu, Y. Zhang, and W. Zhao, Enhanced Spin-Orbit Torque and Multilevel Current-Induced

Switching in W/Co-Tb/Pt Heterostructure, Phys. Rev. Appl. **12**, 044032 (2019).

[23] Y. Fan, P. Upadhyaya, X. Kou, M. Lang, S. Takei, Z. Wang, J. Tang, L. He, L.-T. Chang, M. Montazeri, G. Yu, W. Jiang, T. Nie, R. N. Schwartz, Y. Tserkovnyak, and K. L. Wang, Magnetization switching through giant spin–orbit torque in a magnetically doped topological insulator heterostructure, Nat. Mater. **13**, 699 (2014).

[24] Y. Fan, X. Kou, P. Upadhyaya, Q. Shao, L. Pan, M. Lang, X. Che, J. Tang, M. Montazeri, K. Murata, L.-T. Chang, M. Akyol, G. Yu, T. Nie, K. L. Wong, J. Liu, Y. Wang, Y. Tserkovnyak, and K. L. Wang, Electric-field control of spin–orbit torque in a magnetically doped topological insulator, Nat. Nanotechnol. **11**, 352 (2016).

[25] A. R. Mellnik, J. S. Lee, A. Richardella, J. L. Grab, P. J. Mintun, M. H. Fischer, A. Vaezi, A. Manchon, E. A. Kim, N. Samarth, and D. C. Ralph, Spin-transfer torque generated by a topological insulator, Nature (London) **511**, 449 (2014).

[26] J. Han, A. Richardella, S. A. Siddiqui, J. Finley, N. Samarth, and L. Liu, Room-Temperature Spin-Orbit Torque Switching Induced by a Topological Insulator, Phys. Rev. Lett. **119**, 077702 (2017).

[27] C. Bi, H. Almasi, K. Price, T. Newhouse-Illige, M. Xu, S. R. Allen, X. Fan, and W. G. Wang, Anomalous spin-orbit torque switching in synthetic antiferromagnets, Phys. Rev. B **95**, 104434 (2017).

[28] G. Y. Shi, C. H. Wan, Y. S. Chang, F. Li, X. J. Zhou, P. X. Zhang, J. W. Cai, X. F. Han, F. Pan, and C. Song, Spin-orbit torque in MgO/CoFeB/Ta/CoFeB/MgO symmetric structure with interlayer antiferromagnetic coupling, Phys. Rev. B **95**, 104435 (2017).

[29] Y. Ishikuro, M. Kawaguchi, T. Taniguchi, and M. Hayashi, Highly efficient spin-orbit torque in Pt/Co/Ir multilayers with antiferromagnetic interlayer exchange coupling, Phys. Rev. B **101**, 014404 (2020).

[30] T. Xu, H.-A. Zhou, Y. Dong, Q. Zhang, M. Che, L. Liu, Z. Wu, Z. Guan, L. Yang, and W. Jiang, Fully Compensated Synthetic Antiferromagnets with Pronounced Anomalous Hall and Magneto-Optical Responses, Phys. Rev. Appl. **16**, 044056 (2021).

[31] P. X. Zhang, L. Y. Liao, G. Y. Shi, R. Q. Zhang, H. Q. Wu, Y. Y. Wang, F. Pan, and C. Song, Spin-orbit torque in a completely compensated synthetic antiferromagnet, Phys. Rev. B **97**, 214403 (2018).

[32] S. Pathak and M. Sharma, Polar magneto-optical Kerr effect instrument for 1-dimensional magnetic nanostructures, J. Appl. Phys. **115**, 043906 (2014).

[33] D. A. Allwood, G. Xiong, M. D. Cooke, and R. P. Cowburn, Magneto-optical Kerr effect analysis of magnetic nanostructures, J. Phys. D: Appl. Phys. **36**, 2175 (2003).

[34] N. Nagaosa, J. Sinova, S. Onoda, A. H. MacDonald, and N. P. Ong, Anomalous Hall effect, Rev. Mod. Phys. **82**, 1539 (2010).

[35] M. T. Johnson, P. J. H. Bloemen, F. J. A. den Broeder, and J. J. de Vries, Magnetic anisotropy in metallic multilayers, Rep. Prog. Phys. **59**, 1409 (1996).

[36] Y. Li, X. J. Jin, P. F. Pan, F. N. Tan, W. S. Lew, and F. S. Ma, Temperature-dependent interlayer exchange coupling strength in synthetic antiferromagnetic $[Pt/Co]_2/Ru/[Co/Pt]_4$ multilayers, Chin. Phys. B **27**, 127502 (2018).

[37] M. D. Stiles, Exchange coupling in magnetic heterostructures, Phys. Rev. B **48**, 7238 (1993).

[38] Z. Zhang, L. Zhou, P. E. Wigen, and K. Ounadjela, Angular dependence of ferromagnetic resonance in exchange-coupled Co/Ru/Co trilayer structures, Phys. Rev. B **50**, 6094 (1994).

[39] Y. Yafet, Ruderman-Kittel-Kasuya-Yosida range function of a one-dimensional free-electron gas, Phys. Rev. B **36**, 3948 (1987).

[40] J. Zhao, Y. J. Wang, Y. Z. Liu, X. F. Han, and Z. Zhang, Perpendicular anisotropy dependence of oscillatory interlayer coupling behavior in $[Pt/Co]_5/Ru/[Co/Pt]_5$ multilayers, J. Appl. Phys. **104**, 023911 (2008).

[41] R. Y. Chen, Q. R. Cui, L. Y. Liao, Y. M. Zhu, R. Q. Zhang, H. Bai, Y. J. Zhou, G. Z. Xing, F. Pan, H. X. Yang, and C. Song, Reducing Dzyaloshinskii-Moriya interaction and field-free spin-orbit torque switching in synthetic antiferromagnets, Nat. Commun. **12**, 3113 (2021).

[42] C.-F. Pai, M. Mann, A. J. Tan, and G. S. D. Beach, Determination of spin torque efficiencies in heterostructures with perpendicular magnetic anisotropy, Phys. Rev. B **93**, 144409 (2016).

[43] J. Finley and L. Liu, Spin-orbit-torque Efficiency in Compensated Ferrimagnetic Cobalt-Terbium Alloys, Phys. Rev. Appl.d **6**, 054001 (2016).

[44] J. Sinova, S. O. Valenzuela, J. Wunderlich, C. H. Back, and T. Jungwirth, Spin Hall effects, Rev. Mod. Phys. **87**, 1213 (2015).

[45] P. C. van Son, H. van Kempen, and P. Wyder, Boundary Resistance of the Ferromagnetic-Nonferromagnetic Metal Interface, Phys. Rev. Lett. **58**, 2271 (1987).

[46] O. Hellwig, A. Berger, J. B. Kortright, and E. E. Fullerton, Domain structure and magnetization reversal of antiferromagnetically coupled perpendicular anisotropy films, J. Magn. Magn. Mater. **319**, 13 (2007).

[47] S. Bandiera, R. C. Sousa, S. Auffret, B. Rodmacq, and B. Dieny, Enhancement of perpendicular magnetic anisotropy thanks to Pt insertions in synthetic antiferromagnets, Appl. Phys. Lett. **101**, 072410 (2012).

[48] J. Kim, J. Sinha, M. Hayashi, M. Yamanouchi, S. Fukami, T. Suzuki, S. Mitani, and H. Ohno, Layer thickness dependence of the current-induced effective field vector in Ta vertical bar CoFeB vertical bar MgO, Nat. Mater. **12**, 240 (2013).

[49] K. Garello, I. M. Miron, C. O. Avci, F. Freimuth, Y. Mokrousov, S. Bluegel, S. Auffret, O. Boulle, G. Gaudin, and P. Gambardella, Symmetry and magnitude of spin-orbit torques in ferromagnetic heterostructures, Nat. Nanotechnol. **8**, 587 (2013).

[50] M. Hayashi, J. Kim, M. Yamanouchi, and H. Ohno, Quantitative characterization of the spin-orbit torque using harmonic Hall voltage measurements, Phys. Rev. B **89**, 144425 (2014).